International Journal of Computational Fluid Dynamics, Vol. 20, Nos. 3–4, March–May 2006, 183–192

Taylor & Francis
Taylor & Francis Group

A computational assessment of two arterial switch operations

T. W. H. SHEU†*, S. F. TSAI‡ and I. S. CHIU¶

†Department of Engineering Science and Ocean Engineering, National Taiwan University, No. 1, Sec. 4, Roosevelt Road, Taipei, Taiwan
‡Department of Marine Engineering, National Taiwan Ocean University, Keelung, Taiwan
¶National Taiwan University Hospital, Taipei, Taiwan

Two arterial switch operations (ASO) designed for transposition of great arteries with ventricular septal defect are numerically assessed. To prove that the SRGA (spiral relationship of the normally related great arteries) arterial switch operation (ASO) is hemodynamically superior to that of the Lecompte procedure, three-dimensional Navier–Stokes simulations were carried out in the resulting two different vessels. In the mixed tri-quadratic finite element formulation, the streamline upwind model developed on the sup–inf-satisfying elements is employed to enhance convective stability. For the sake of accuracy, the degree of upwinding needed to enhance stability is analytically derived on the one-dimensional basis. For quantitative assessment of the two investigated operations, we calculate the pressure on the vessel surface and the wall shear stress from the simulated velocities. It is found that SRGA surgery is accompanied with lower pressure and higher shear stress, in comparison with those obtained from the Lecompte operation. Additionally, SRGA surgery results in much smaller areas of high pressure and low shear stress. Evidence is also given to show that the SRGA manoeuvre is less susceptible to stenosis. We also show that SRGA is the operation of choice for the ASO from the energy point of view since this anatomy is associated with smaller total energy loss coefficient and hydraulic dissipated power index.

Keywords: ASO; TGA; SRGA; Lecompte; Mixed tri-quadratic finite element; Streamline upwind model

1. Introduction

Transposition of great arteries (TGA) is a common congenital heart disease. The abnormal aorta arises from the right ventricle and the pulmonary artery from the left ventricle. Surgical correction needs to be performed to sustain the patients' life. A septal defect, another congenital abnormality of heart in the fetus, permits abnormal blood circulation from the left (high pressure) side of the heart to the right (low pressure) side. The resulting excessive blood flow through the lung can cause pulmonary hypertension and heart failure.

The Lecompte procedure (Lecompte *et al.* 1981) has long been the standard arterial switch operation (ASO) surgery designed for patients with transposition of great arteries and ventricular septal defect (VSD). An ASO involves closure of atrial and ventricular septal defects, excision and then the removal of coronary ostia. The surgery is followed by removing the pulmonary artery bend, reinserting the right coronary artery, and reorienting the aortic segment, which is placed behind the pulmonary bifurcation. Surgical operation is completed by anastomosing the aorta, reinserting the left coronary artery and, finally, performing anastomosis of the pulmonary outflow tract (Lecompte *et al.* 1981). This technically demanding and difficult operation avoids use of prosthetic conduit to reconstruct the pulmonary outflow tract (Lecompte *et al.* 1982). Additionally, the heart anatomy remains the same as that of a normal person after the operation. There still existed, however, reports that the anterior location of the pulmonary arteries is a potential cause of the right ventricular outflow obstruction for patients who have undergone the Lecompte manoeuver. Flattening of the main pulmonary artery, compression of the aorta, and the resulting reduction of cross-sectional areas are also known to be the direct outcome of the ASO with the Lecompte manoeuvre. As a result, there is room for operation improvement to avoid branch pulmonary stenosis.

*Corresponding author. Tel.: +886-2-33665791. Fax: +886-2-23929885. Email: twhsheu@ntu.edu.tw

International Journal of Computational Fluid Dynamics
ISSN 1061-8562 print/ISSN 1029-0257 online © 2006 Taylor & Francis
http://www.tandf.co.uk/journals
DOI: 10.1080/10618560600803056

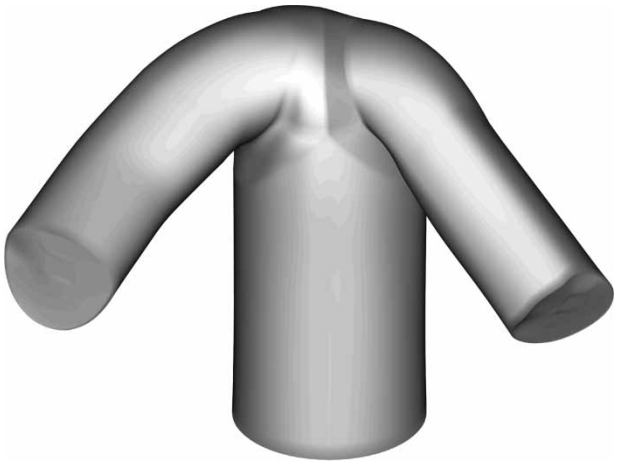

Figure 1. Schematic of the vessel model for the Lecompte manoeuver.

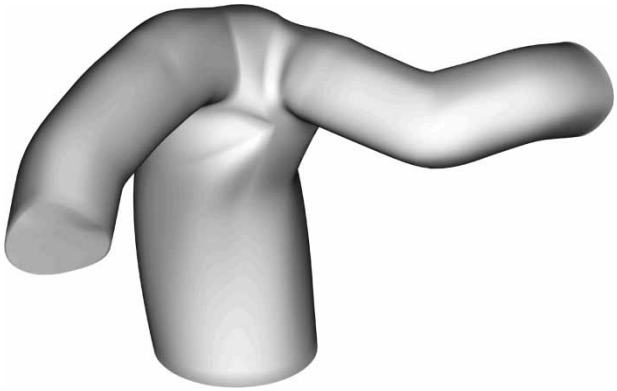

Figure 2. Schematic of the vessel model for the spiral artery switch operation.

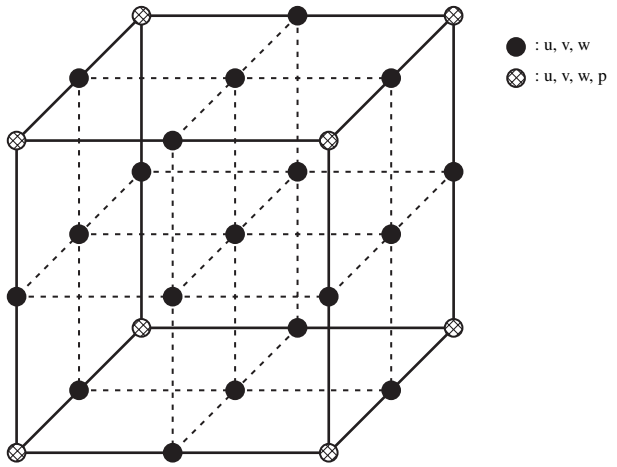

Figure 3. Schematic of the storage points for $\underline{u}$ and p in the tri-quadratic element.

From March 1998 to October 1999, twelve congenital patients underwent complete transposition of the great arteries at the National Taiwan University Hospital. All survived after the ASO with the modified Lecompte manoeuver, known as the SRGA (Chiu *et al.* 2000).

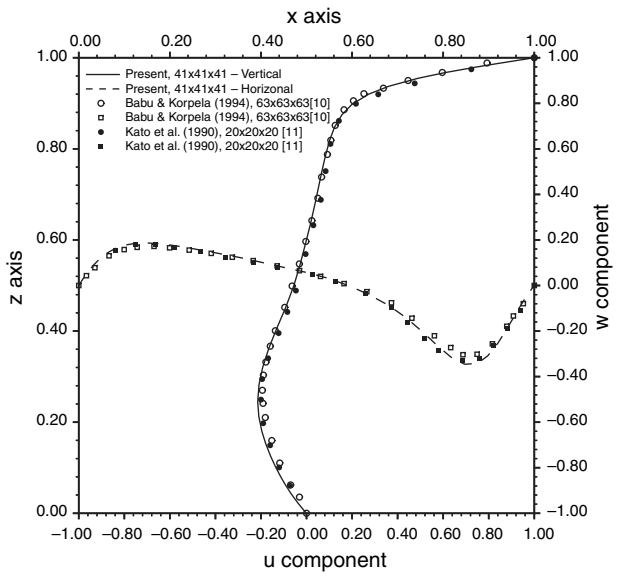

Figure 4. Comparison of the simulated mid-plane velocities in the cavity.

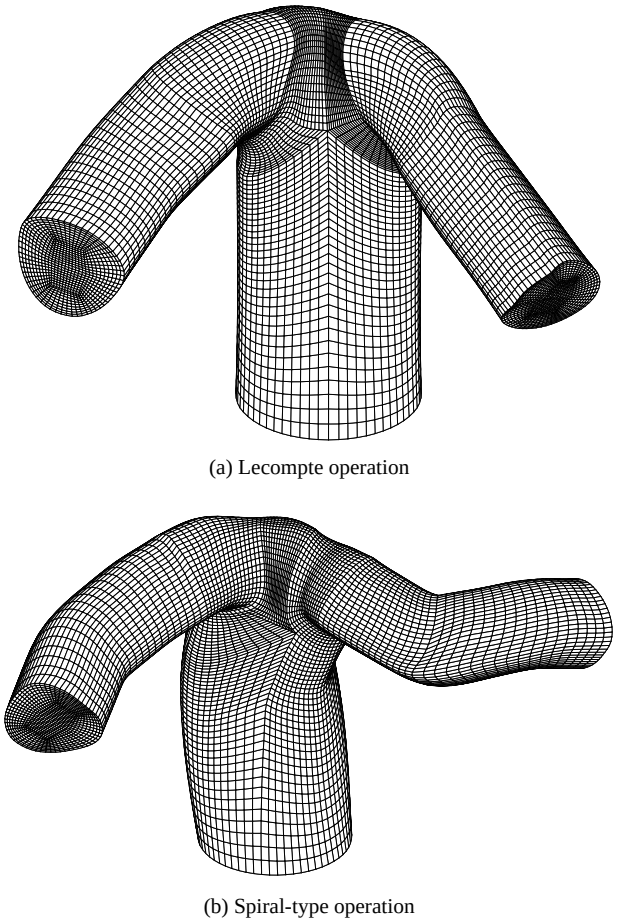

(a) Lecompte operation

(b) Spiral-type operation

Figure 5. Surface meshes for the two investigated ASO vessel models.

To reduce the possibility of pulmonary stenosis, the spiral relationship of the normally related great arteries (SRGA) operation involves a spirally reorientating the aortic and pulmonary arteries. The right pulmonary artery becomes

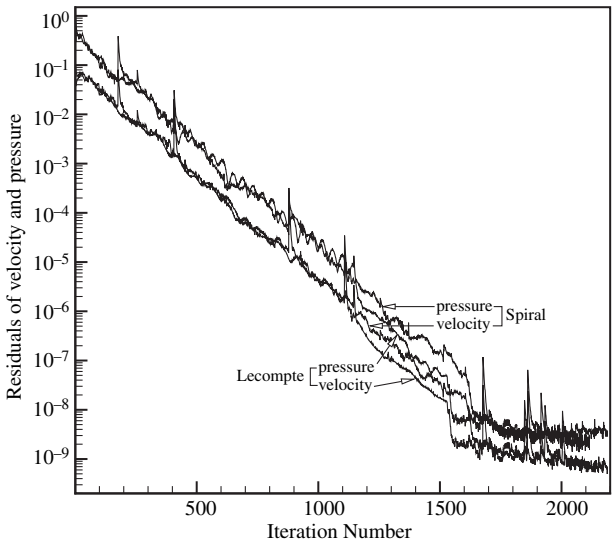

Figure 6. The plots of residual reduction against iteration for the two investigated vessel models.

slightly twisted backward and is placed behind the aorta artery. This spiral reorientation of arteries results in an anatomic correction which resembles the normal anatomy. With the successful practice of SRGA, we are motivated to provide evidence that the SRGA operation is superior to the Lecompte operation from a hemodynamic point of view. Assessment of two ASOs was conducted based on the simulated pressure and shear stress on the vessel surface. We also provide evidence to show that SRGA is less liable to stenosis in the pulmonary artery. For quantitative evaluation, two surgical procedures are also assessed from the energy point of view. The total energy loss coefficient and the hydraulic dissipated power index (Low *et al.* 1993) can be calculated from the simulated three-dimensional Navier–Stokes solutions.

In the present work, the working equations in primitive variables, subject to the prescribed boundary conditions for pressure, are described in section 2. This is followed by the presentation of three-dimensional mixed finite element model employed to simulate the

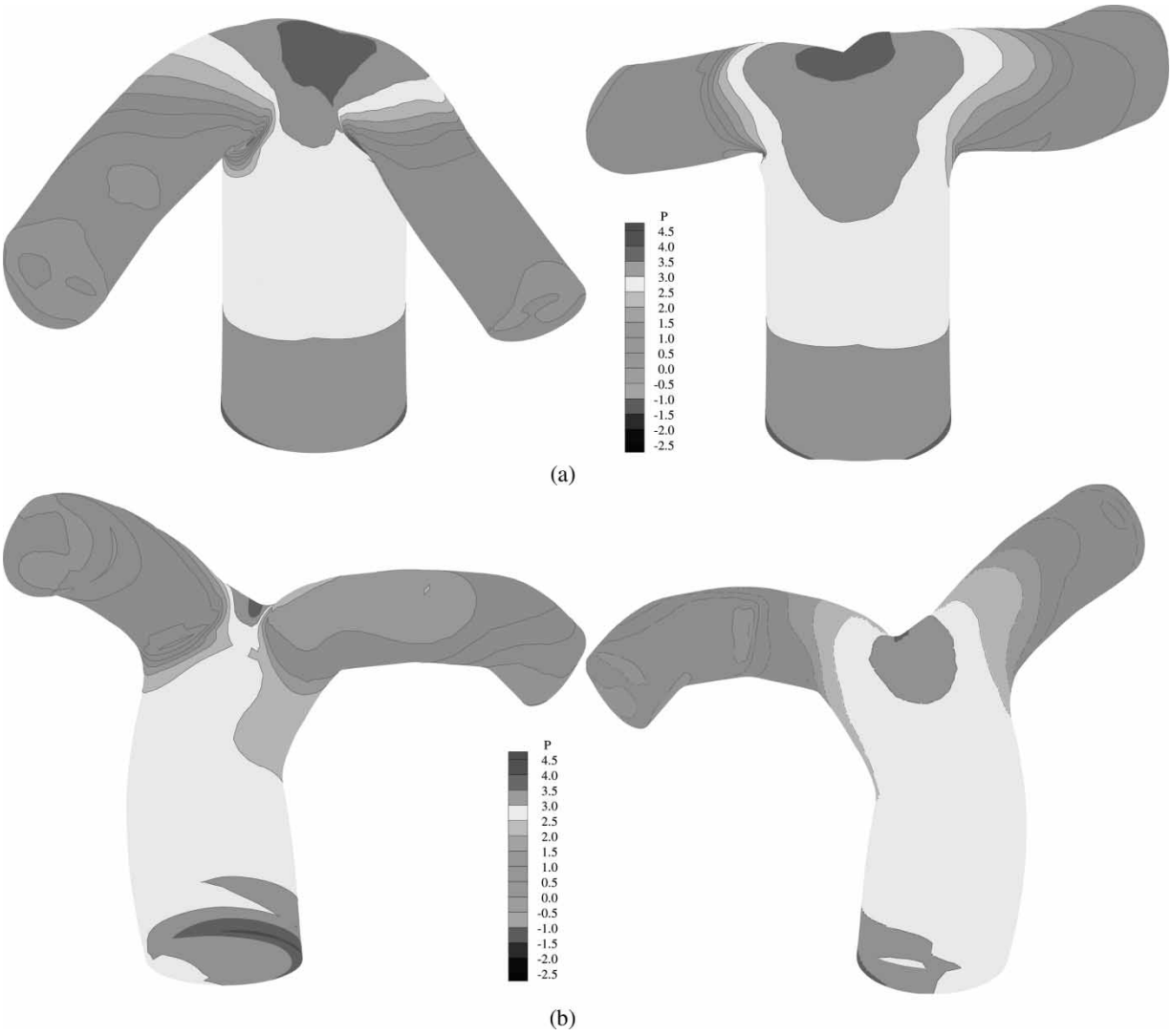

Figure 7. The simulated pressure contours on the vessel walls seen from different views: (a) Lecompte ASO operation; (b) SRGA ASO operation.

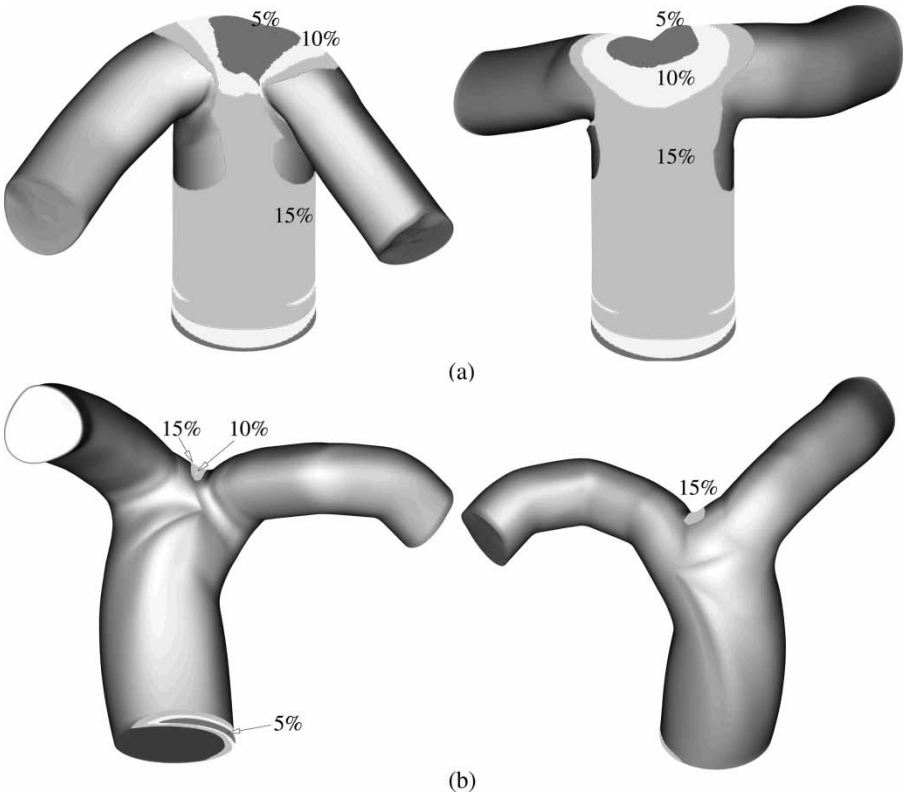

Figure 8. The plots of wall surface pressures with their highest magnitudes (at three levels), which are marked with different shaded colors. (a) Lecompte ASO operation; (b) SRGA ASO operation.

transport of blood flow in the vessel. For the sake of stability, the test function is properly chosen so that the discrete stability along the streamline direction can be enhanced by the added stabilized term. For the sake of accuracy, the locally analytic one-dimensional scheme is employed to solve the convection-diffusion equation. The integrity of employing the streamline upwind finite element model on quadratic elements will be demonstrated. In section 3, the vessel configurations and flow conditions are detailed. In section 4, two ASO operations will be numerically assessed from the hemodynamic and energy viewpoints. Investigation into the blood flow is addressed on the formation of secondary and reversed flows. By virtue of the topology theory, the Lecompte ASO operation is shown to result in a clinically undesirable separated flow. Finally, we provide concluding remarks in section 5.

2. Numerical model

Numerical modeling of blood flow in the anatomies schematic in figures 1 and 2 requires solving the three-dimensional viscous flow equations. Under the incompressible and steady-state assumptions for the present hemodynamic analyses, the continuity and Navier–Stokes equations in Cartesian coordinates are represented as follows:

$$\frac{\partial u_i}{\partial x_i} = 0, \tag{1}$$

$$\frac{\partial}{\partial x_m}(u_m u_i) = -\frac{\partial p}{\partial x_i} + \frac{1}{Re}\frac{\partial^2 u_i}{\partial x_m \partial x_m}. \tag{2}$$

The currently employed steady-state assumption is unusual in arterial studies (Dubini *et al.* 1999) and the effect of flow pulsatility is left for future investigation. The above elliptic differential system for the velocity vector $\underline{u}$ and pressure p is sought subject to the rigorous Dirichlete-type boundary condition $\underline{u} = \underline{g}$ (Ladyzhenskaya 1963), where

$$\int_\Gamma \underline{n}\cdot\underline{g}\,\mathrm{d}\Gamma = 0.$$

For the sake of generality, all the lengths are normalized by the hydraulic diameter of the blood vessel l_{ref}, and the velocity components u_{ref} by the mean inlet velocity. The Reynolds number is, thus, defined as $Re = (u_{\mathrm{ref}} l_{\mathrm{ref}})/\nu$, where ν is the kinematic viscosity of the blood flow. Another assumption made in this study is that the flow is

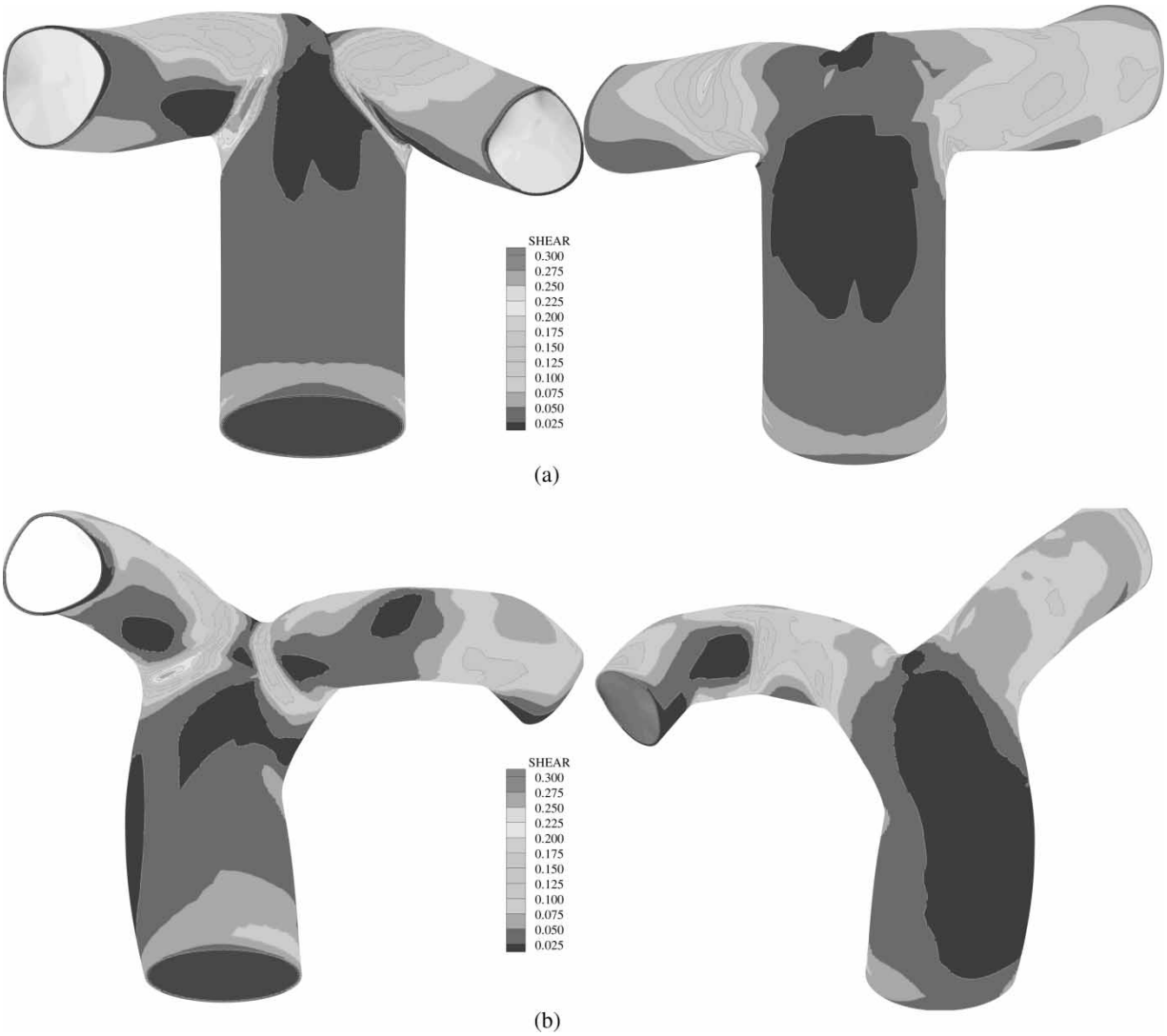

Figure 9. The simulated shear stress on the vessel walls. (a) Lecompte ASO operation; (b) SRGA ASO operation.

laminar. This simplification is clinically plausible for a large arterial vessel, with the exception for blood flow in the proximal aorta and the aortic arch (Caro *et al.* 1978, Nichols & O'Rourke 1990, Ethier *et al.* 1999). Calculations performed under the rigid wall condition are also acceptable since the vessel compliant nature is generally known to have a modest impact on the wall shear stress (Steinman & Ethier 1994, Perktold & Rappitsch 1995).

Given the admissive functions $\underline{w} \in H_0^1(\Omega) \times H_0^1(\Omega)$ and $q \in L_0^2(\Omega)$ in a simply-connected domain Ω, field variables $\underline{u} \in H_0^1(\Omega)$ and $p \in L_0^2(\Omega)$ are sought from the weighted residuals statement given below

$$\int_\Omega (\underline{u}\cdot\nabla)\underline{u}\cdot\underline{w}\,\mathrm{d}\Omega + \frac{1}{Re}\int_\Omega \nabla\underline{u} : \nabla\underline{w}\,\mathrm{d}\Omega - \int_\Omega p\nabla\cdot\underline{w}\,\mathrm{d}\Omega = \int_{\Gamma/\Gamma_n} r\underline{w}\cdot\underline{n}\,\mathrm{d}\Gamma + \int_{\Gamma/\Gamma_\gamma} \underline{s}\cdot\underline{w}\times\underline{n}\,\mathrm{d}\Gamma, \tag{3}$$

$$\int_\Omega (\nabla\cdot\underline{u})q\,\mathrm{d}\Omega = 0. \tag{4}$$

Equation (3) involves surface integration along $\Gamma/\Gamma_{n,r}$, which denotes the complement of $\Gamma_{n,r}$ in $\Gamma = \partial\Omega$. By definition, $\underline{\phi} \in \Gamma/\Gamma_i$ $(i = n,\ r)$ means that $\underline{\phi} \in \Gamma$ and $\underline{\phi} \notin \Gamma_i$. In the above, $\underline{n}$ denotes the unit outward vector normal to Γ. In equation (3), $r = -p + (1/Re)\underline{n}\cdot\nabla\underline{u}\cdot\underline{n}$ and $\underline{s} = \frac{1}{Re}\underline{n}\cdot\nabla\underline{u}\times\underline{n}$.

The chosen basis functions for approximating $(\underline{u}, p)$ are critical in the mixed finite element simulation of incompressible flow equations. The LBB (or inf–sup) condition is normally considered as the guiding principle of choosing basis spaces (Babuska 1971, Brezzi & Douglas 1988). Since the element schematic in figure 3, which involves tri-quadratic polynomials, N^i $(i = 1 \sim 27)$, for the velocities and tri-linear polynomials, M^i $(i = 1 \sim 8)$, for the pressure, accommodates the inf–sup div-stability condition, this element pair will be used in the present study.

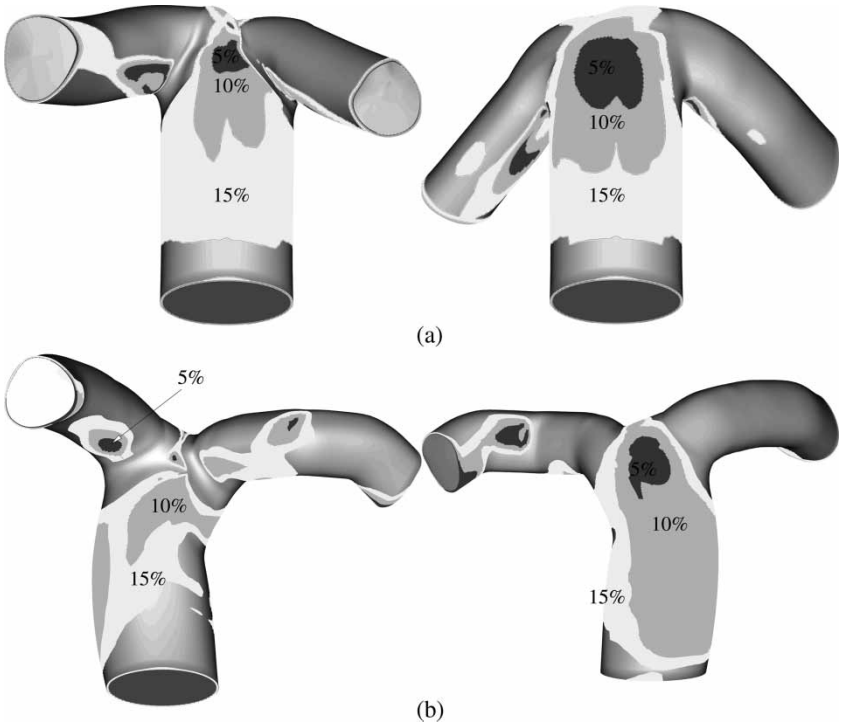

Figure 10. The plots of wall surface shear stresses with their lowest magnitudes (at three levels), which are marked with different shades. (a) Lecompte ASO operation; (b) SRGA ASO operation.

Prediction of blood flows having a Peclet number (or cell Reynolds number) larger than two requires careful stabilization of advective terms shown in the momentum equations. Enhancement of convective stability can be accomplished by adding a biased polynomial to the shape function (Hughes 1979). The nodal values at the upwind side, while being favorably considered, the resulting equation is prone to numerical contamination due to false diffusion errors (Patankar 1980) introduced in the analysis of multi-dimensional advection-diffusion equation. To reduce the crosswind diffusion error without sacrificing the convective stability, we developed the streamline operator on quadratic elements (Sheu *et al.* 2000).

Within the mixed finite element context, the required computer time and storage may be excessive. For this reason, the Lanczos-based BiCGSTAB iterative solver (Van de Vorst 1992) is employed to circumvent the problem with irregular convergence in the calculation of unsymmetric matrix equations. Other reasons for favoring the BiCGSTAB stem from its ability to minimize the simulated residuals through GMRES(1) and avoid the transpose matrix. For computational efficiency, the element-by-element capability has been built into this modern iterative solver (Wang and Sheu 1997). As is usual, the integrity of the developed three-dimensional Petrov–Galerkin finite element code for incompressible flow equations is validated by solving the lid-driven cavity problem at $Re = 400$. The simulated results in figure 4 show good agreement with the mid-plane velocity profiles of Kato *et al.* (1990) and Babu and Korpela (1994).

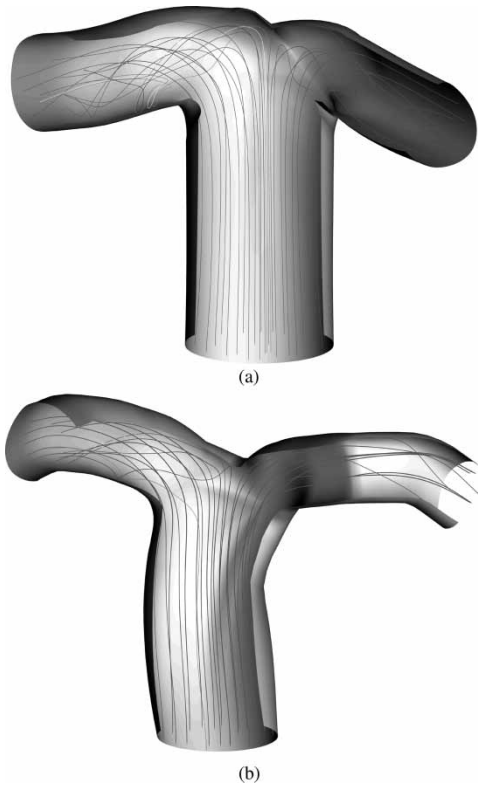

Figure 11. The simulated particle trajectories for the two investigated arteries. (a) Lecompte ASO operation; (b) SRGA ASO operation.

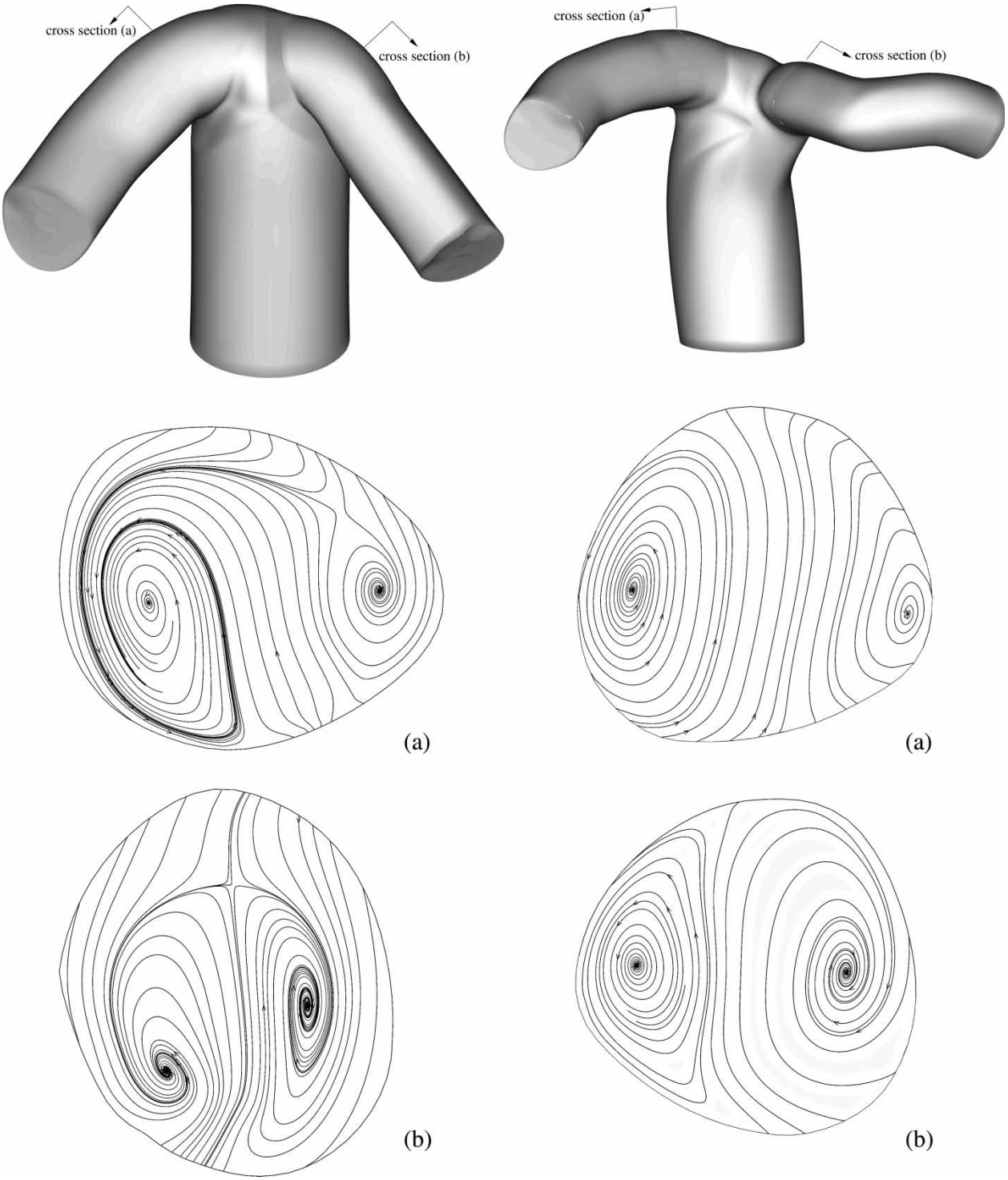

Figure 12. Plots of the secondary flow patterns at some selected cutting planes immediately downstream of the vessel bifurcation.

Table 1. The simulated blood volume rates, together with their distributions on the left side, Q_{L_o}, the right side, Q_{R_o} and the mean velocities for analyses conducted in the Lecompte and spiral models.

	Q_i	Q_{L_o} (%)	Q_{R_o} (%)	$\bar{u}_i$	$\bar{u}_{L_o}$	$\bar{u}_{R_o}$
Lecompte	2.907	1.704 (58.6%)	1.203 (41.4%)	1.0	1.3573	1.1805
Spiral	2.905	1.720 (59.2%)	1.185 (40.8%)	1.0	1.3691	1.1518

Table 2. The simulated extreme pressures, maximum shear force, and energetic indices, C_e and $\dot{W}_{diss}$, for analyses conducted in the Lecompte and spiral models.

	Δp ($p_{max} - p_{min}$)	Shear force τ(max)	$\dot{W}_{diss}$	C_e
Lecompte	5.979	0.9004	6.796	4.748
Spiral	4.648	0.2631	6.085	4.252

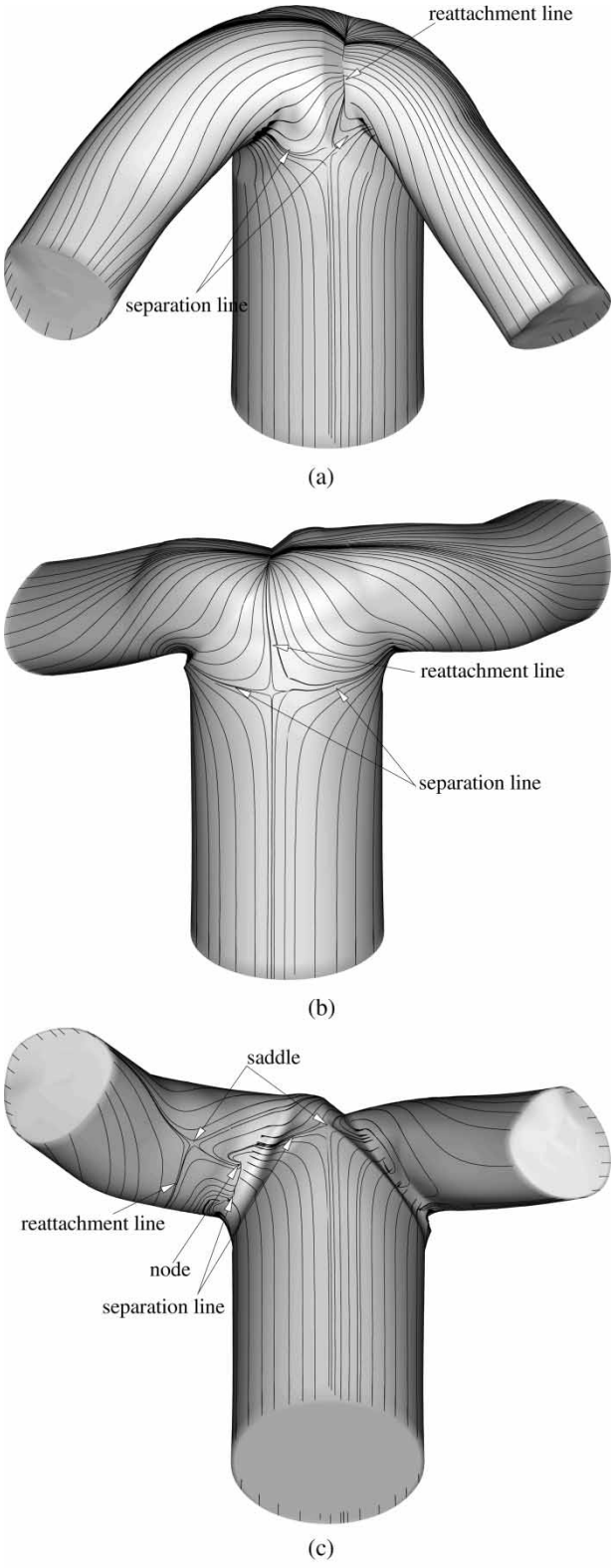

Figure 13. Different views of the simulated critical lines plotted on the Lecompte vessel walls.

3. Problem description

The blood vessels under current investigation are schematically shown in figures 1 and 2, respectively. The Reynolds number for the investigated laminar blood flow was 295, based on the blood viscosity $\nu = 2.83 \times 10^{-6}\,\mathrm{m^2\,s^{-1}}$ ($\nu = (\mu/\rho)$, where $\rho = 1060\,\mathrm{kg\,m^{-3}}$ and $\mu = 3 \times 10^{-3}\,\mathrm{Pa\,s}$) and the prescribed inlet flow rate $\dot{Q} = 0.8\,\mathrm{l\,min^{-1}}$. Since the prediction quality is greatly dependent on the mesh quality, it is desirable to generate grids as smooth as possible. To avoid excessively distorted grids in the bifurcation vessels schematic in figures 1 and 2, the physical domain is discretized on a multi-block basis. Within 24 blocks, 112,585 mesh points shown in figure 5 are generated. It is noted that grids are refined in regions immediately adjacent to the vessel walls as well as in regions having a marked change in configuration.

To close the differential system of working equations, boundary conditions prescribed on the inlet plane, two outlets, and the vessel walls are required. At a given flow rate, we assumed that the blood at the inlet plane was fully-developed. At the truncated exit planes, pressure values are prescribed according to the lumped-parameter model of Leval *et al.* (1988):

$$p_i = p_{\mathrm{LA}} + R_{\mathrm{lung}}\dot{Q}_i \quad (i = \mathrm{LPA},\ \mathrm{RPA}). \tag{5}$$

In the above, R_{lung} and $\dot{Q}_i$ denote the lung resistance to the blood flow and the simulated flow rate during the iteration, respectively.

4. Computed results

Blood flow dynamics in branching vessels is highly complex and can exhibit many nonlinear features rarely seen in the classical benchmark problem. A question arises as to whether the simulated finite element solutions are convergent. For this reason, we plot in figure 6 the predicted residuals against nonlinear iterations to demonstrate that the results to be discussed are indeed convergent. The effectiveness of two investigated ASOs can be judged from different viewpoints. In the following, the two operations will be hemodynamically assessed.

A successful ASO operation requires small and uniform pressure on the vessel wall so as to avoid impairment of the vessel wall for follow-up patients. This motivates us to plot in figures 7 and 8 the pressure contours. A close examination of the simulated pressure contours reveals that SRGA outperforms the Lecompte operation. The high pressure region shown in figure 8(a) is smaller in size and the wall pressure is smaller in magnitude than those shown in figure 8(b).

Another key factor which can determine the long-term success or failure of ASO is the wall shear stresses. The shear stress of smaller magnitude has been hypothesized to be the hemodynamic risk factor for various vascular diseases. The region with low shear stress is susceptible to intimal thickening. The accompanying undesirable long particle residence time is the natural mechanism for the low density lipoprotein to accumulate in the intima (Ku *et al.* 1985, Fry 1987). In view of the importance of wall shear stresses in the vascular surgery, we plot in figures 9 and 10 the stress distributions on the investigated two

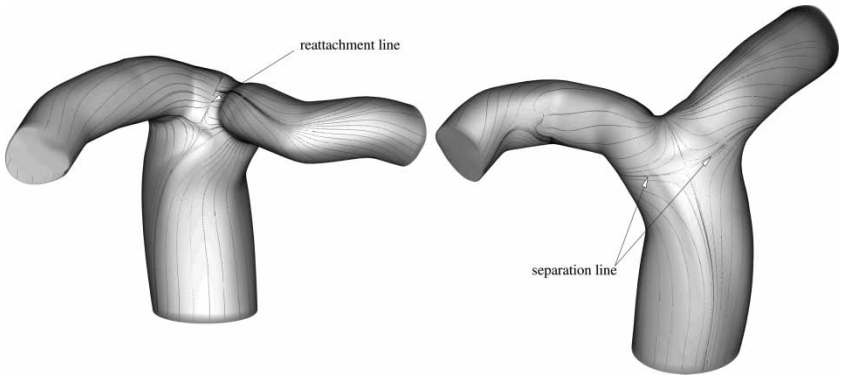

Figure 14. Different views of the simulated critical lines plotted on the SRGA vessel walls.

vessel walls. It can be seen from figure 10 that the Lecompte operation results in shear stresses that are larger in size but are smaller in magnitude. The implication is that the Lecompte manoeuver is prone to stenosis and atherosclerotic lesion, as compared to that for the spiral-type ASO operation.

To demonstrate that flow reversal is the main feature found in the blood vessel, the trajectories of the seeded particles at the upstream side are plotted in figure 11. Unlike the simulated pathlines in the spiral-type blood vessel, flow reversal is the main hemodynamic signature found in the Lecompte ASO operation. In view of the greater probability that blood will be entrained into the reversed flow region, the refined spiral ASO surgery is believed to have a better hemodynamic performance. Coincident with the reversed flow development is the formation of secondary flow in regions downstream of the vessel bifurcation. As blood particles move towards the branching region, they are subjected to centrifugal acceleration, which can cause the blood to propagate more rapidly towards the outer vessel wall. As a result, the secondary flow is quickly intensified. Figure 12 shows that the secondary flow developed immediately downstream of the bifurcated region is much more complicated due to complex interaction of secondary and reversed flows. This interacting structure persists to the downstream exit. The secondary flow proceeds counterclockwise along the inner vessel wall while it is being pushed outward through the core region. The larger velocity is, thus, found near the outer vessel wall.

Besides the hemodynamic consideration, assessment of the investigated ASOs can be made from an energy viewpoint. The physical quantities which have been frequently employed are the total energy loss coefficient C_e and the hydraulic dissipated power $\dot{W}_{diss}$, defined as (Dubini *et al.* 1996)

$$C_e = \frac{\left(\frac{1}{2}\rho V_i^2 + p_i\right)Q_i - \sum_j \left(\frac{1}{2}\rho V_j^2 + p_j\right)Q_j}{\frac{1}{2}\rho V_i^2 Q_i}, \quad (6)$$

$i = \text{inlet},\ j = \text{LPA, RPA},$

and

$$\dot{W}_{diss} = \left(\frac{1}{2}\rho V_i^2 + p_i\right)Q_i - \sum_j \left(\frac{1}{2}\rho V_j^2 + p_j\right)Q_j, \quad (7)$$

$i = \text{inlet},\ j = \text{LPA, RPA}.$

In the above, p_i (i = LPA,RPA) denotes the mean blood pressure obtained at each inlet/exit plane. The C_e and $\dot{W}_{diss}$ tabulated in tables 1 and 2 are the convincing evidences of favorably considering the spiral ASO surgery. The prevailing flow reversal in the Lecompte vessel is deemed to be responsible for having larger values of C_e and $\dot{W}_{diss}$.

Due to the influence of separated flow on the hemodynamic performance of ASO surgery, it is worthwhile to determine where the blood flow is separated and is then reattached to the vessel wall. For this reason, the topological theory is employed as a technique to depict lines of separation and reattachment on the irregular three-dimensional vessel wall. Following the terminology of Legendre (1956), as in our previous studies (Chiang *et al.* 2000, Sheu *et al.* 2000), the critical lines are plotted in figures 13 and 14. The Lecompte vessel is seen to be marked by lines of separation and reattachment in the region downstream of the vessel bifurcation. The tendency of observing entrainment flow in the recirculating region and its subsequent flow obstruction in the branching region becomes higher.

5. Concluding remarks

In this paper, the Navier–Stokes equations for incompressible blood flow has been solved for numerically assessing the two investigated ASOs. The conclusions drawn from this study were under the physical assumption that the flow was laminar and steady. From the hemodynamic point of view, the ASO with the spiral manoeuver is superior to the Lecompte operation based on the simulated shear stress and pressure. The present three-dimensional finite element simulation has revealed the undesirable low shear stress and high pressure in

the Lecompte operation. From the energy point of view, the spiral-type ASO is also the better choice because of its resulting lower total energy loss coefficient and hydraulic dissipated power. It has also been found that the hemodynamic structure is far more complicated than expected, with the coexistence of secondary and recirculating flow patterns. The observed flow reversal is deemed to be responsible for the stenosis formed in the proximity of bifurcation. The blood flow separation and reattachment regions have been investigated through the theoretical topology study.

Acknowledgements

Financial support from the National Science Council of the Republic of China under Grant NSC94-2915-I-002-027 is acknowledged.

References

Babu, V. and Korpela, S.A., Numerical solution of the incompressible three-dimensional Navier–Stokes equations. *Comput. Fluids*, 1994, **23**(5), 675–691.

Babuška, I., Error bounds for finite element methods. *Numer. Math.*, 1971, **16**, 322–333.

Brezzi, F. and Douglas, J., Stabilized mixed methods for the Stokes problem. *Numer. Math.*, 1988, **53**, 225–235.

Caro, C.F., Pedley, T.J., Schorter, R.C. and Seed, W.A., *The Mechanics of the Circulation*, 1978 (Oxford University Press: Oxford).

Chiang, T.P., Sheu, T.W.H. and Wang, S.K., Side wall effects on the structure of laminar flow over a plane-symmetric sudden expansion. *Comput. Fluids*, 2000, **29**(5), 467–492.

Chiu, I.S., Wu, S.J., Chen, M.R., Lee, M.L., Wu, M.H., Wang, J.K. and Lue, H.C., Modified arterial switch operation by spiral reconstruction of the great arteries in transposition. *Ann. Thorac. Surg.*, 2000, **69**, 1887–1892.

de Leval, M.R., Kilner, P., Gewiling, M. and Bull, C., Total cavopulmonary connection: a logical alternative to atriopulmonary connection for complex Fontan operation. *J. Thorac. Cardiovasc. Surg.*, 1988, **96**(5), 682–695.

Dubini, G., de Leval, M.R., Pietrabissa, R., Montevecchi, F.M. and Fumero, R., A numerical fluid mechanical study of repaired congenital heart defects application to the total cavopulmonary connection. *J. Biomech.*, 1996, **29**(1), 111–121.

Dubini, G., Migliavacca, F., Pennati, G., Pietrabissa, R., Fumero, R. and de Leval, M.R., Haemodynamics of the reconstrcution of complex cardiac malformations. In *Haemodynamics of the Arterial Organs*, edited by X.Y. Xu and N.W. Collins, pp. 1–41, 1999 (WIT Press: Southampton).

Ethier, C.R., Steinman, D.A. and Ojah, M., Comparisons between computational hemodynamics, photochromic dye flow visualization and magnetic resonance velocimetry. In *Haemodynamics of Arterial Organs*, edited by X.Y. Xu and N.W. Collins, pp. 131–183, 1999 (WIT Press: Southampton).

Fry, D.L., Mass transport, atherogenesis and risk. *Arteriosclerosis*, 1987, **7**, 88–100.

Hughes, T.J.R., *Finite Element Methods for Convection Dominated Flows, AMD*, **34**, 1979 (ASME: New York).

Kato, Y., Kawai, H. and Tanahashi, T., Numerical flow analysis in a cubic cavity by the GSMAC finite-element method. *JSME Int. J. Series II*, 1990, **33**, 649–658.

Ku, D.K., Giddens, D.P., Zarins, C.K. and Glagov, S., Pulsatile flow and atherosclerosis in the human carotid bifurcation, positive correlation between plaque location and low oscillating shear stress. *Arteriosclerosis*, 1985, **5**(3), 293–302.

Ladyzhenskaya, O.A., *Mathematical Problems in the Dynamics of a Viscous Incompressible Flow*, 1963 (Gordon and Breach: New York).

Lecompte, Y., Zannini, L., Hazan, E., Jarreau, M.M., Bex, J.P., Tu, T.V. and Neveux, J.Y., Anatomic correction of transposition of the great arteries. New technique without use of a prosthetic conduit. *J. Thorac. Cardiovasc. Surg.*, 1981, **82**, 629–631.

Lecompte, Y., Neveux, J.Y., Leca, F., Zannini, L., Tu, T.V., Duboys, Y. and Jarreau, M.M., Reconstruction of the pulmonary outflow tract without prosthetic conduit. *J. Thorac. Cardiovasc. Surg.*, 1982, **84**, 727–733.

Legendre, R., Séparation de courant Íéconlment laminaire tridimensional. *Rech. Aéro*, 1956, **54**, 3–8.

Low, H.T., Chew, Y.T. and Lee, C.N., Flow studies on atriopulmonary and cavopulmonary connections of the Fontan operations for congenital heart defects. *J. Biomed. Eng.*, 1993, **15**, 303–307.

Nichols, W.W. and O'Rourke, M.F., *McDonald's Blood Flow in Arteries*, 3rd ed., 1990 (Lea & Febiger: Philadephia).

Patankar, S.V., *Numerical Heat Transfer and Fluid Flow*, 1980 (Hemisphere: Washington, DC).

Perktold, K. and Rappitsch, G., Computer simulation of local blood flow and vessel mechanics in a compliant carotid artery bifurcation model. *J. Biomech.*, 1995, **28**(7), 845–856.

Sheu, T.W.H., Wang, M.M.T. and Tsai, S.F., Element by element parallel computation of incompressible Navier–Stokes equations in three dimensions. *SIAM J. Sci. Comput.*, 2000, **21**(4), 1387–1400.

Steinman, D.A. and Ethier, C.R., Numerical modelling of flow in a distensible end-to-side anastomosis. *ASME J. Biomech. Eng.*, 1994, **116**, 295–301.

Van der Vorst, H.A., BI-CGSTAB: a fast and smoothly converging variant of BI-CG for the solution of nonsymmetric linear systems. *SIAM J. Sci. Stat. Comput.*, 1992, **13**(2), 631–644.

Wang, M.M.T. and Sheu, T.W.H., An element-by-element BiCGSTAB iterative method for three-dimensional steady Navier–Stokes equations. *J. Comput. Appl. Math.*, 1997, **79**, 147–165.